MOLECULAR SPINTRONICS DEVICES EXHIBITING PROPERTIES OF A SOLAR CELL

Pawan Tyagi[1,2], Christopher Riso[1]

[1]Mechanical Engineering, University of the District of Columbia, Washington, DC, 20008, USA
[2]Chemical and Materials Engineering, University of Kentucky, Lexington, Kentucky-40506, USA
Email:ptyagi@udc.edu

ABSTRACT:

Almost all the solar cell created so far are based on electronic charge. This paper reports a photovoltaic effect based on the spin property of electrons. This spin-based photovoltaic effect was observed on magnetic tunnel junction based molecular spintronics devices (MTJMSD). MTJMSDs were produced by covalently bonding organometallic molecular clusters (OMCs) between the top and bottom ferromagnetic electrodes of Co/NiFe/AlOx/NiFe magnetic tunnel junctions along the exposed side edges. The MTJMSD configuration, which showed the photovoltaic effect, also exhibited OMC induced strong antiferromagnetic coupling (Ref. Tyagi et al., 2015, Nanotechnology, Vol. 26, p. 305602) and room temperature current suppression (Ref. Tyagi et al., 2019, Organic Electronics, Vol, 64, p. 188-194). Our MTJMSD were fabricated below 100 °C temperature and employed earth-abundant transition metals like nickel and iron. This paper shows that MTJMSD's photovoltaic effect was susceptible to the magnetic field, temperature, and light intensity. The solar cell efficiency was estimated to be ~3%. Our MTJMSD approach provides a mass-producible platform for harvesting solar energy and open a myriad of opportunities to incorporate photogenerated charges for the logic and memory operation in the molecular spintronics devices.

INTRODUCTION

The spin-photovoltaic cell is a brand-new field of interest where light absorption and power generation are dependent on magnetic properties of electrodes and spin properties of the electron. Spin-photovoltaic cells are exciting because new physics can be utilized to generate solar electricity. More importantly, spin-photovoltaic cells can be economically fabricated by the utilization of many earth-abundant materials, such as iron(Fe), nickel(Ni) and cobalt(Co). Initially, the spin-photovoltaic effect was theoretically predicted around 1991[1, 2]. The first category of spin-based photovoltaic cells focused on utilizing conventional charge-based p-n junction photovoltaic cell platform. In the theoretical studies, the conventional p-n junction was made spin sensitive by magnetic doping [3, 4] or by applying a magnetic field [5]. The second category of spin-photovoltaic cells focus on the quantum transport. Many theoretical studies have predicted the spin-photovoltaic effect in quantum transport via quantum wires and nanoscale channels [1, 6-8]. However, experimental efforts and progress have been insignificant in the above mentioned two categories of the spin- photovoltaic effects. Interestingly, many experimental studies have demonstrated the spin-photovoltaic effect in rather uncommon systems. Bottegoni et al. [9] utilized circularly polarized light to produce two spatially well-defined electron populations with opposite in-plane spin projections in the nonmagnetic semiconductor/metal system. The spatial separation of opposite spins was achieved by modulating the phase and amplitude of the light wavefronts entering in a germanium semiconductor layer covered with a patterned platinum metal overlayer. However, utilization of polarized light for observing spin-photovoltaic effect creates potential issues with regards to practical applications of spin-based solar cells in direct sun radiation, which is naturally unpolarized. Sun et al.[10] have utilized unpolarized light radiation to produce a spin-photovoltaic effect with a system of NiFe/C_{60}/AlOx/Cobalt(Co) based spin valves. In this work, the light was absorbed by the C_{60} molecular film sandwiched between two ferromagnetic electrodes. This system yielded a spin- photovoltaic effect and was sensitive towards the direction of the magnetic moment of the ferromagnetic electrodes that were weakly coupled via the C_{60} and AlOx layer.

In this paper, we demonstrate the spin-photovoltaic effect on molecule-based spintronic devices that were produced by utilizing ferromagnetic metals like NiFe, and Co. We observed the spin-photovoltaic

effect on a magnetic tunnel junction (MTJ) with exposed side edges (Fig. 1a) that was transformed into a molecular device (Fig.1b). In our case, paramagnetic molecules were covalently bonded with two ferromagnetic leads of the MTJ along the exposed edges (Fig.1b). The magnified view of a single molecule connection with two ferromagnets is shown in Fig. 1c. Our molecular device has the following three distinctions with respect to prior work by Sun et al. [10]: (a) Our molecular device is formed by covalently bonding molecular array across the tunnel barrier of Co/NiFe/AlOx/NiFe tunnel junctions along the edges (Fig. 1b). Whereas Sun et al. [10] sandwiched the C_{60} molecules between Co and NiFe. (b) We have used a paramagnetic molecule that produced extremely strong exchange coupling between the ferromagnetic electrodes leading to a significant change in magnetic properties and transport properties [11, 12]. Whereas in Sun et al. work [10] the magnetic coupling was supposedly insignificant because it was not discussed separately. We refer to our MTJ based molecular spintronics device (MSD) as MTJMSD in this paper. Here we report the observation of a photovoltaic effect on our MTJMSD using unpolarized white light at room temperature. We also report magnetic force microscopy(MFM), Kelvin probe atomic force microscopy (KPAFM), and Raman studies of the MTJMSDs to provide a comprehensive understanding and a potential mechanism behind the observed spin-dependent photovoltaic effect.

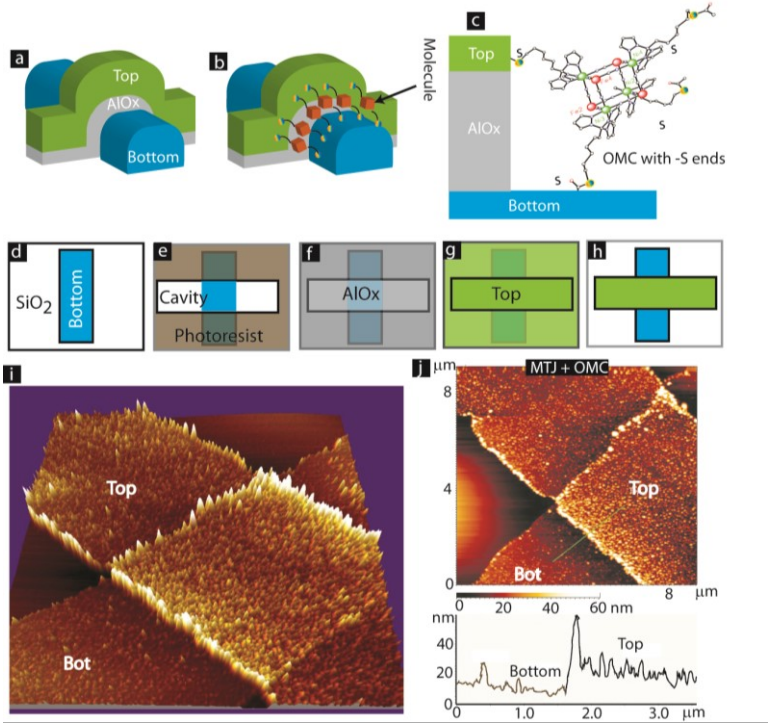

Fig.1: 3D view of an MTJ with exposed side edges (a) before and (b) after bridging molecular channels between ferromagnets. (c) Magnified view of OMC paramagnetic molecule covalently bonded to ferromagnets via thiol bonding. Fabrication of MTJMSD involve (d) bottom electrode deposition on insulating substrate, (e) photolithography for the deposition of (f) ~ 2 nm AlOx insulator and (g) top ferromagnet, followed by (h) liftoff. AFM of an MTJ (i) before and (j) after hosting hosting OMC channels.

EXPERIMENTAL DETAILS:

MTJ for the observation of photovoltaic effect were deposited on oxidized silicon with 300 nm silicon dioxide layer. MTJ thin-film configurations, Ta(2-5 nm)/Co(5-7 nm)/NiFe(3-5 nm)/AlOx(2 nm) /NiFe(10-12 nm) were produced by the liftoff method (Fig. 1d-h). This method involves depositing the bottom electrode on an insulating substrate (Fig. 1d) followed by the photolithography to produce a cavity in the photoresist to produce a cross junction (Fig. 1e). In the photoresist's cavity, ~2 nm AlOx (Fig. 1f) and top ferromagnetic electrode (Fig. 1g) were deposited. Liftoff of the photoresist produced a tunnel junction with exposed side edges (Fig. 1h). OMC was covalently bonded across the tunnel junction to form MTJMSD. Detailed MTJMSD fabrication protocol has been published elsewhere [13-17]. Typically, bottom and top electrodes were ~5 µm each and hence cross junction area was ~25 μm^2. The 3D atomic force microscope (AFM) image before treating an MTJ with OMC is shown in Fig. 1i. This MTJ remained intact after the interaction with OMCs (Fig. 1i); the physical height difference between the top and bottom ferromagnet did not change after the treatment with OMCs(Fig. 1j). OMC's thiol functional groups formed covalent bonding with the NiFe layers to produce molecular exchange coupling that dominated over the weak coupling via the AlOx tunneling barrier. This OMC coupling impacted the magnetic properties of the MTJMSDs.[11] An OMC possessed cyanide-bridged octametallic molecular cluster, $[(pzTp)Fe^{III}(CN)_3]_4$-

$[Ni^{II}(L)]_4[O_3SCF_3]_4$ [(pzTp) = tetra(pyrazol-1-yl)borate; L = 1-S(acetyl)tris(pyrazolyl)decane] chemical structure and was paramagnetic in nature[18]. The HOMO-LUMO gap for the cubic core was theoretically calculated to be 0.33 eV; also the Ni and Fe atoms of each core were ferromagnetically coupled [19]. The spin-dependent photovoltaic effect was observed on at least ten MTJMSDs that were produced in four different batches. Transport studies of the MTJMSD were performed with a Keithley 2430 1kW pulse source meter and Keithley 6430 sub-Femtoamp source meter. White light radiation was supplied from a halogen lamp (Microlite FL 3000), The spectra of Microlite FL 3000 was characterized by Ocean Optics Spectrometers (Model S4000). We also used NaioFlex AFM, Picoscan AFM to conduct MFM. For KPAFM study, we utilized Cr/gold- coated cantilever that was produced by Budget Sensor®. For MFM study, we utilized Co coated Nanoscience Nanosensor® brand magnetized PPP-MFMR AFM cantilevers. Raman study was performed with JASCO NRS-4100 using 785 nm laser. During Raman study laser power, accumulation period, and exposure time were optimized.

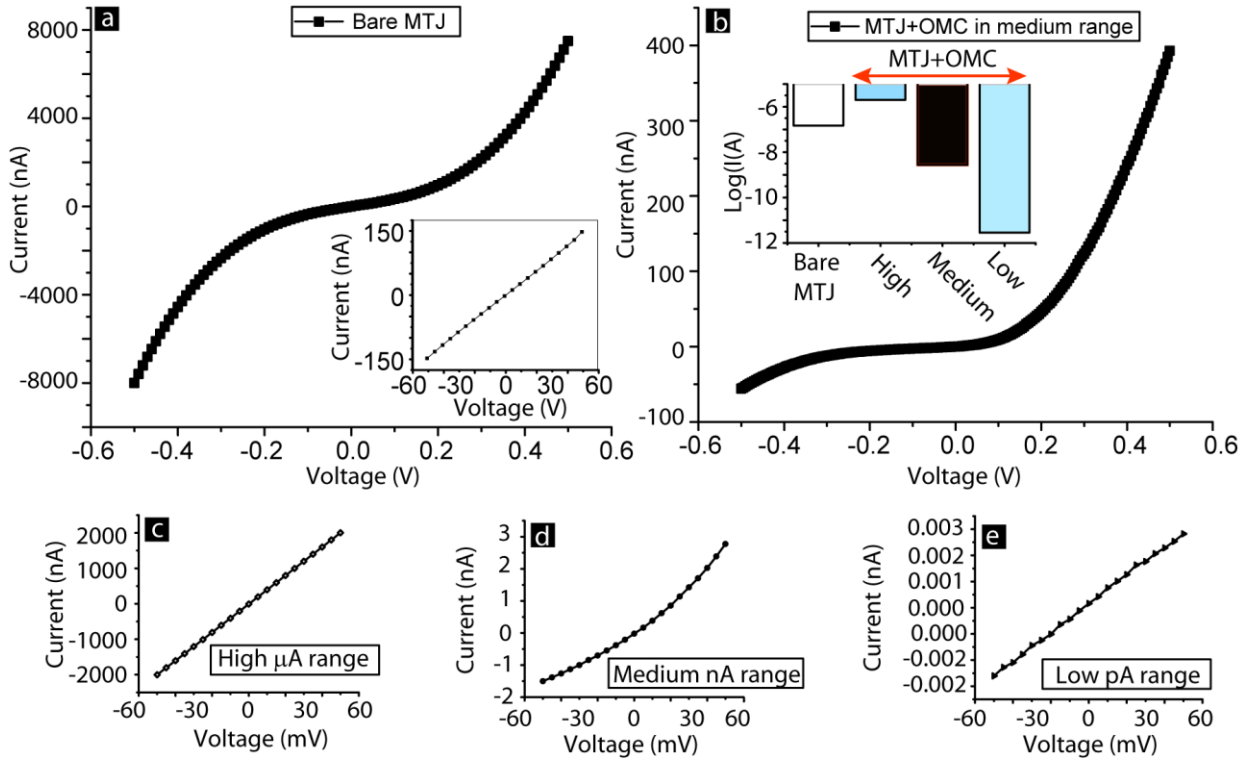

Fig. 2: Transport study of (a) bare MTJ showing tunneling type transport, inset show current magnitude for low voltage range. (b) After hosting OMCs as transport channels MTJMSD shifted among high low and medium current state, medium current state was the most stable state and showed diode like response. Low voltage current response of MTJMSD in (c) high, (d) medium, and (e) suppressed current state.

RESULTS AND DISCUSSION:

We investigated the photovoltaic effect on a wide range of tunnel junction based molecular devices with different metal electrodes and molecules [14, 17, 20]. However, the spin-dependent photovoltaic effect was only observed with MTJMSD utilizing Ta/Co(5-7 nm)/NiFe(3-5 nm)/AlOx(2 nm)/NiFe(10 nm) MTJs and paramagnetic OMC. The Co/NiFe bilayer ferromagnetic films exhibited higher coercivity as compared to NiFe top electrode. Hence, even though OMC bonded with two NiFe layers present in the top and bottom electrodes but, the magnetic property of the bottom NiFe layer was affected by the Co. The hysteresis loop for Co/NiFe was ~four times wider than that of top NiFe [11]. Ta only served as a seed layer to promote adhesion. A typical MTJ exhibited non-linear current-voltage graph indicating that ~2 nm AlOx insulating barrier produced expected tunneling type transport characteristics between two

ferromagnetic electrodes (Fig. 2a). However, after the bridging of OMCs between two ferromagnetic electrodes of the MTJ, in the manner shown in Fig. 1c, effective MTJMSD transport varied from µA to pA range at room temperature (inset Fig. 2b). MTJMSDs' transport appeared in three broad categories that can be identified as a high current state (in µA range at 50 mV, Fig. 2c), medium current state (nA range at 50 mV, Fig. 2d), and low current state (pA range at 50 mV, Fig. 2e). Out of these three current states medium and low current states, are termed as representative of suppressed current states; the magnitude of MTJMSD's current in medium (Fig. 2e) and low current states (Fig. 2e) were three to six orders of magnitude smaller than the magnitude of current observed at bare MTJ (Fig. 2a).

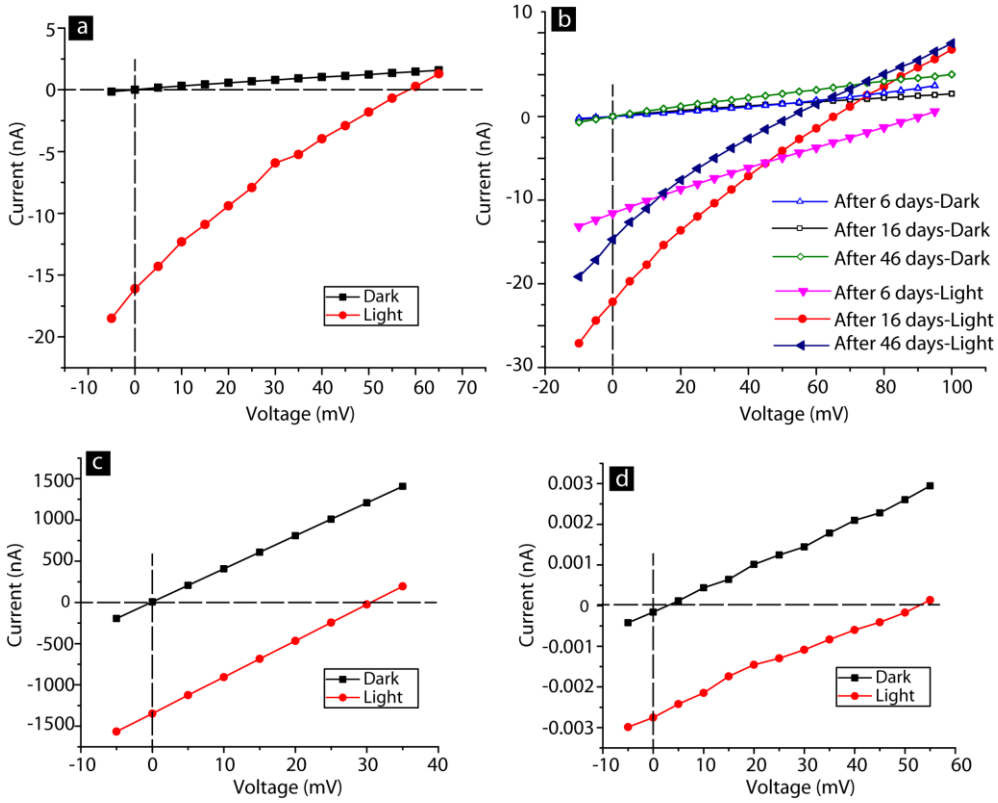

Fig. 3: MTJMSD's Photovoltaic effect in (a) middle current range. (b) Effect of time on photovoltaic response in middle current range MTJMSD's photovoltaic effect in (c) µA high current and (d) pA level suppressed current state.

A bare MTJ by itself did not respond to light. It mainly responded to light after getting transformed into an MTJMSD and attaining a suppressed current state. In our prior publications, we have discussed the observation of current suppression [13, 20]. Here we briefly mention the current suppression in the context of spin-photovoltaic effect. We explained that such a large change in transport properties was associated with the OMC induced changes in the basic magnetic properties of the MTJs. We have also investigated and published a number of magnetic studies on MTJMSD[11, 12]. Magnetic studies were critical in showing that MTJMSDs' current suppression was associated with equally dramatic changes in the OMC induced magnetic properties [11]. Multiple magnetic studies gave direct evidence that OMCs created long-range changes in the magnetic properties of bare MTJs, and the ferromagnetic leads used therein [11, 12]. OMCs produced very strong antiferromagnetic exchange coupling that impacted the ferromagnetic electrode at room temperature. OMC effect was confirmed by three independent magnetic measurement techniques, namely SQUID magnetometer, Ferromagnetic Resonance, and MFM. For the magnetic study, we utilized an array of ~7000 MTJ/samples to confirm the OMCs impact. Observation of OMC impact on

~7000 MTJ, with the same Ta/Co(5-7 nm)/NiFe(3-5 nm)/AlOx(2 nm)/NiFe(10 nm) thin-film configuration as used in this paper, suggested that ferromagnetic films of the MTJMSD have attained new properties. However, in the previous work, we only discussed transport and magnetic properties[11-13, 20]. This paper is elaborating on the photovoltaic effect on the same MTJMSDs.

We found that the medium current state, when MTJMSD was in the nA level current state, was more stable and produced the relatively stable photovoltaic response (Fig. 3a). This current state appears after several hours of incubating MTJMSD. Photovoltaic effect on the MTJMSD in the medium current range was time-sensitive (Fig. 3b); however, this variation in photo-current was insignificant as compared to the magnitude of current variation between high (Fig. 3c) and suppressed current states (Fig. 3d). The photovoltaic response of the MTJMSD in the medium current state over 46 days showed that three measurements were still in 10-25 nA range (Fig. 3b). The open-circuit voltage varied from 50-110 mV range. Such a time-dependent change in MTJMSD's photovoltaic response is associated with the molecule induced magnetic ordering around the MTJMSD. We have discussed the effect of the MTJMSDs' magnetic orderings and their impact on transport properties elsewhere in this paper. We have also observed changes in MTJMSD transport and photoresponse in the high and low current states discussed in Fig. 3c-d. Both high and low current states ended up settling in the medium current level.

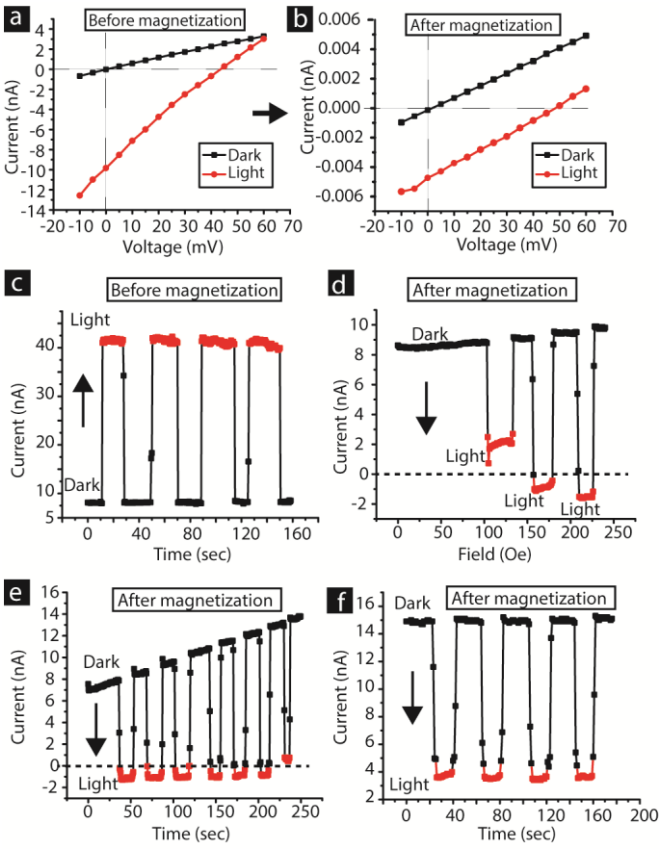

Fig. 4: Typical MTJMSD's photovoltaic effect (a) before and (b) after magnetization. A freshly produced MTJMSD showing (c) photo response with time before magnetization. (d) Same MTJMSD showing transitory photovoltaic response under varying magnetic field after magnetization. (e) MTJMSD's photovoltaic response without magnetic field 13 min after study shown in (d). (f) MTJMSD after 35 min of the study shown in panel (e).

In the initial state, MTJMSDs' transport could be perturbed from medium nA current level to ~μA range by conducting multiple current-voltage studies or magnetoresistance study at a fixed voltage and by applying the magnetic field varying gradually up to ~300 Oe (Fig. 2). Such cases have been discussed in the prior work without a discussion on MTJMSDs' photoresponse, which is the focus of this paper [13, 20]. The photovoltaic effect of an MTJMSD that attained a temporary high current state is shown in Fig. 3c. On this MTJMSD sample, the high current state appeared after conducting multiple current-voltage studies. The unstable representative photoresponse in MTJMSD's high current state is shown in Fig. 3c. More importantly, a slight change in open-circuit voltage (Voc) was observed. However, this high current state invariably changed to more stable several orders of magnitude lower suppressed current states; most frequently observed stable current state was an nA range medium current level. Typically, a transition from nA medium current level to pA level low current level at room temperature occurred during the magnetization of MTJMSD under ~0.2 T permanent magnetic field [13, 20]. During magnetization, no current was forced through the device. Due to the application of magnetic field photocurrent reduced by ~3 orders of magnitude (Fig. 3d) as compared to the stable nA level medium current state (Fig. 3a). In such cases, the photovoltaic effect produced ~pA photovoltaic current (Fig. 3d).

Impact of magnetic field on MTJMSD's transport suggested that the photovoltaic effect is dependent on the spin property of the electron. For the sample discussed here, Voc changed from ~30 mV in the nA level medium current range to ~55 mV (Fig. 3d).

We studied the effect of magnetic on MTJMSD's photovoltaic response. Typically, application of the in-plane magnetization moved an MTJMSD from its nA level medium current state to the suppressed current state (Fig. 4a-b). For the case discussed in Fig. 4a, before in-plane magnetization Isc was tens of nA and Voc was ~45 mV. However, after the magnetization, the same MTJMSD settled in the pA level suppressed current state and exhibited three orders small Isc, and ~50 mV Voc. We believe that during magnetization MTJMSD, magnetic electrodes are reorganized to yield a suppressed current state. On one MTJMSD sample, we had an opportunity to study the change in photoresponse with time because this sample did not settle in pA state right after the magnetization, as expected in general. This specific MTJMSD's photovoltaic effect exhibited higher sensitivity towards the magnetic field in the initial state, or within the first few days after MTJMSD formation. The response of light and the magnetic field is discussed in an MTJMSD that was studied two days after the MTJMSD fabrication. Photoresponse was studied at 50 mV bias and by turning 96 W/m^2 white light on and off before and after MTJMSD magnetization by the ~0.2 T permanent magnetic field. We chose 50 mV bias to investigate if Voc changes significantly with respect to typically observed ~50 mV (Fig. 4a-b). Before the magnetization, this MTJMSD was in the nA level medium current range (Fig. 4c). This MTJMSD exhibited >4 folds current increase under light radiation (Fig. 4c). Interestingly, the direction of photogenerated current reversed after the magnetization step (Fig. 4d-f). Within 10 minutes after the magnetization by the permanent magnet, the sample was subjected to varying in-plane magnetic field, and photoresponse was recorded (Fig. 4d). Under the varying magnetic field, MTJMSD's photocurrent shifted from net positive to net negative. Such a change in the photocurrent sign suggests that the magnitude of open-circuit voltage (Voc) was shifting. To generate net positive current Voc should be < 50 mV, at Voc=50 mV photocurrent is expected to be 0. When net photocurrent became negative, Voc shifted to become more than 50 mV (Voc> 50 mV) (Fig. 4d). Interestingly, the dark current did not change at the same rate as photocurrent did with the magnetic field (Fig. 4d).

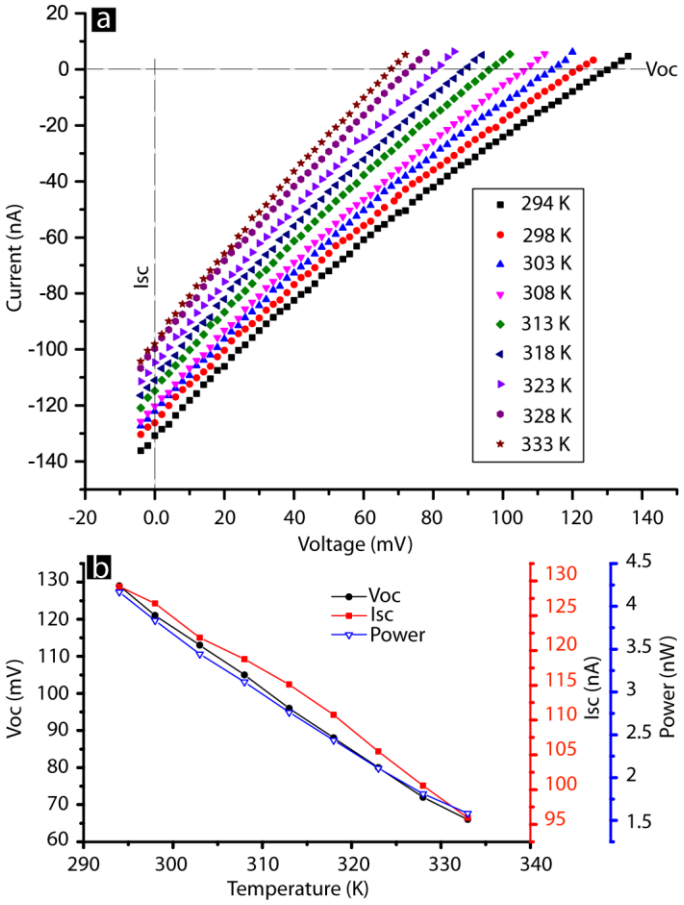

Fig. 5: (a) Effect of temperature on MTJMSD's transport. (b) Effect of temperature on open circuit voltage (Voc), saturation current (Isc), and power.

To further investigate the stability of net negative photocurrent, we studied photoresponse without varying magnetic field (Fig. 4e). Interestingly, the dark current kept increasing with time at a much faster rate than photocurrent (Fig. 4e); this is a reverse order as compared to the scenario in (Fig. 4d). After ~200 sec during the study, the photocurrent switched back to become net positive (Fig. 4e). We surmised that increase in dark current and change in photocurrent with time was due to MTJMSD approaching an

equilibrium magnetic ordering with time. Increase in MTJMSD's dark current is associated with the decrease in angle between the magnetization vectors of the two ferromagnets.[21] We assume that the OMC impacted ferromagnetic electrodes tending to stabilize with time. As mentioned in this paper, an MTJMSD has two 5 µm wide and ~10 nm thick ferromagnetic electrodes connected by ~10000 OMCs. We tried to understand the MTJMSD's dependency on time via Monte Carlo simulations. During our Monte Carlo simulations, we noted that the size of ferromagnetic electrodes directly affects the time required to reach in the equilibrium state.[11] However, actual MTJMSD is too big to simulate, and hence, we do not have an exact estimation of equilibrium time. We conducted a photoresponse study after 35 minutes (Fig.4f). As expected, MTJMSD exhibited stable dark current and a stable net positive photocurrent (Fig. 4f). It is also noteworthy that the starting current level of each study was close to the endpoint of the prior study (Fig. 4c-f). It means that in this experiment, MTJMSD did not go too far away from the equilibrium state after the magnetization. However, in general, we were only able to see the dramatic change in the MTJMSD current after the magnetization under the permanent magnetic field (Fig. 4b).

Besides, we were unable to influence MTJMSD's photovoltaic effect with a small magnetic field. We were unable to maneuver the direction of magnetization of the ferromagnetic leads in the MTJMSD's stable suppressed current state. The reason was that OMC produced an extremely strong exchange coupling between MTJMSD's magnetic lead that could not be overcome by the small magnetic field. As discussed elsewhere in this paper, three independent magnetic measurements confirmed that OMC produced very strong antiferromagnetic coupling between the ferromagnetic electrodes [11]. Application of 3T magnetic field was unable to overcome the OMC induced exchange coupling at 150 K [11]. Also, experimental and theoretical studies showed that OMC induced exchange coupling strength was ~450 K range that is almost half of the inter-atomic exchange coupling strength [11]. Due to this strong OMC induced antiferromagnetic coupling ferromagnetic electrodes are expected to be aligned antiparallel to each other.

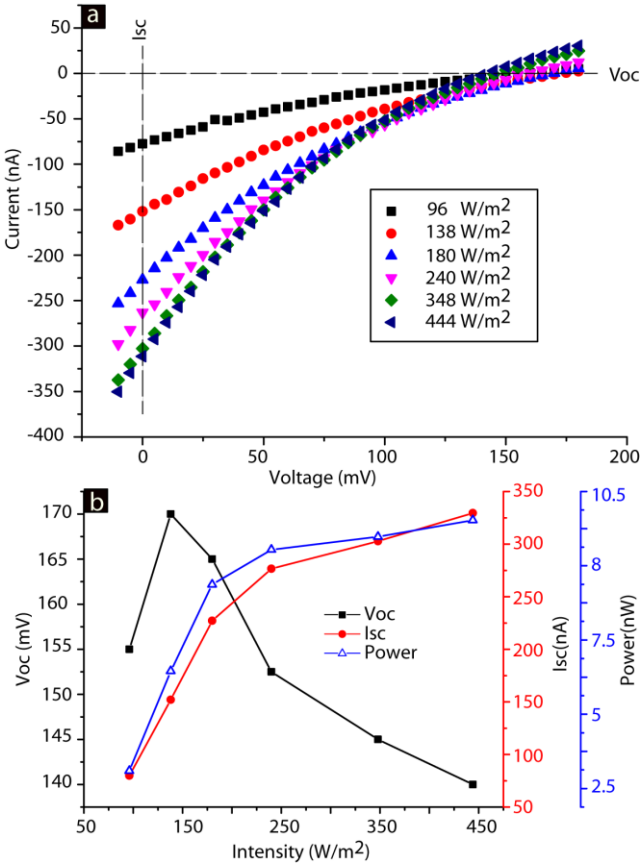

Fig. 6: (a) Effect of white light intensity on MTJMSD's transport. (b) Effect of light intensity on open circuit voltage (Voc), saturation circuit current (Isc), and power

It is noteworthy that OMCs did not produce a photovoltaic effect on nanomagnetic tunnel junctions where nonmagnetic gold leads were utilized [22]. In addition, exposed tunnel junction edges where photo-active CuPc molecules were placed between two gold metal electrodes did not yield any photovoltaic effect or power generation [23]. Similarly, light-sensitive ~15 nm active molecular layer sandwiched between carbon electrodes did not produce measurable spin-dependent photovoltaic effect [24].

MTJMSD's photovoltaic effect is associated with magnetic materials and spin properties of the electrode. We further investigated MTJMSD's photovoltaic effect under varying light intensity and temperature. Variation in temperature significantly impacted the photocurrent and Voc (Fig. 5a). For this study temperature varied from 294 K to 333 K. This temperature range was selected to avoid the irreversible impact of temperature on magnetic leads and disturbance to MTJMSD's current state. It is noteworthy that magnetic electrodes start oxidizing at a high rate after ~360 K [15]. For this study light intensity was maintained at 96 W/m^2. Open circuit voltage (Voc) reduced from 129 mV to 66 mV linearly with temperature (Fig. 5b). On the other hand, the saturation current (Isc) under light radiation decreased linearly from 129 nA to 95 nA when temperature increased from 294 K to 333 K (Fig. 5b). For the calculation of power generated at MTJMSD, we assumed ~0.25 fill factor. We calculated the power by multiplying fill factor, Isc, and Voc (Fig. 5b). The power generated at MTJMSD decreased linearly with temperature (Fig. 5b). We have discussed the efficiency aspect elsewhere in this paper. Power decreased by ~2.7 nW/K rate. This trend is like the one seen in the conventional p-n junction solar cells [25]. It is worth noting that MTJMSD's current in the darkness increased exponentially with temperature. Utilizing the dark current vs. temperature data suggested that MTJMSD's thermal activation energy barrier was ~82±11 mV. Hence, the impact of temperature on MTJMSD was significantly different in the dark (exponential scale) and light (linear scale).

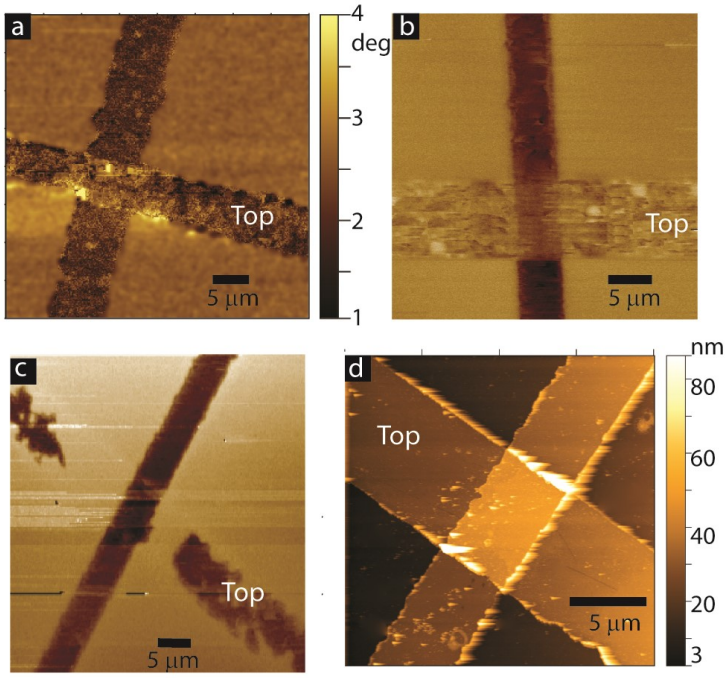

Fig. 7: Magnetic force microscopy (MFM) in (a) µA level high current state, (b) in low current state, and (c) in medium current state. Topographical AFM image of the junction shown in panel (c).

We also studied the effect of the light intensity on MTJMSD's photovoltaic effect (Fig. 6a). However, as compared to the effect of temperature, the effect of light intensity was more prominent on saturation current at zero voltage (Isc) (Fig. 6a). We also estimated the amount of energy reaching on the MTJMSD cross-section (Fig. 6a). The current-voltage graph for each light intensity is shown in Fig. 6a. As the light intensity increased the Voc first increased and then kept decreasing (Fig. 6b). Voc peaked around ~117 W/cm^2 (Fig. 6b). Whereas, Isc initially increased linearly with light intensity increasing from 96 to 139 W/cm^2 (Fig. 6b), and they tend to increase at a reduced rate. Like Fig. 4c, we calculated power by assuming a fill factor (FF) of 0.25. The power is calculated to discuss the MTJMSD's energy conversion efficiency. For 444 W/m^2 light intensity, the corresponding light intensity on an MTJMSD of 25 µm^2 area was 11 nW (Fig. 6b). However, the power generated at the MTJMSD was 11.5 nW. This estimation suggests that power generated from the junction is more than the incident light radiation power. This estimate suggested the photovoltaic power is generated from an area that is bigger than the typical tunnel junction area at the cross junction. To investigate this hypothesis, we investigated the OMC impact range on the MTJMSD. We mainly conducted magnetic force microscopy (MFM) on the MTJMSD cross junctions. MFM has been successful in capturing the OMC induced magnetic changes in pillars of several hundred MTJs of the similar thin-film configurations [11].

In the high current state, an MTJMSD exhibited the same magnetic color (Fig. 7a). Also, MFM of the bare MTJ exhibited similar color for the top and bottom electrodes. However, in low pA level current state, the top and bottom magnetic electrodes exhibited distinct color contrasts (Fig. 7b). Interestingly, in the nA level medium current state MFM study showed that a significant part of the top ferromagnetic layer lost magnetic contrast near junction vicinity (Fig. 7c). The loss of magnetic contrast around junction was not due to and physical damage of the top NiFe electrode. Topography image of the junction area in Fig.7c showed that top magnetic NiFe layer was physically intact (Fig. 7d). We observed that the disappearance of magnetic contrast near the MTJ junction area was a prevalent feature of the MTJMSDs reported in this paper. The OMC impacted regions near junctions are expected to be in an equilibrium state with the bulk of the ferromagnetic electrodes. We are unable to calculate the lower and upper bound of the OMC affected NiFe electrode regions. However, according to the MFM image (Fig.7b-c) several tens of μm were affected by OMC beyond the junction area. To estimate the MTJMSD light to electricity conversion efficiency, we utilized the MFM image shown in Fig. 7c. We assumed that the OMC impacted top ferromagnetic electrode area near MTJMSD junction in Fig. 7c represents the photoactive area for the nA level medium current state and responsible for the spin photovoltaic effect. The area of the full length of the top electrode shown in Fig. 7c was estimated to be 385 μm^2. As discussed elsewhere in this paper, the MTJMSD produced 11.5 nW under 444 W/m^2 light radiation. Using 385 μm^2 area yielded ~7 % energy conversion efficiency in the nA level medium current state. However, if we included, both top and bottom electrodes near MTJMSD as the photosensitive area, then the photosensitive area turned out to be ~730 μm^2. Utilizing ~730 μm^2 area for estimation yielded ~3.5% energy conversion efficiency. Our estimates of photoactive regions are based on simple assumptions that may be quite different than the actual area responsible for power generation. Further studies are required to perform an accurate estimate of MTJMSD's photoactive areas.

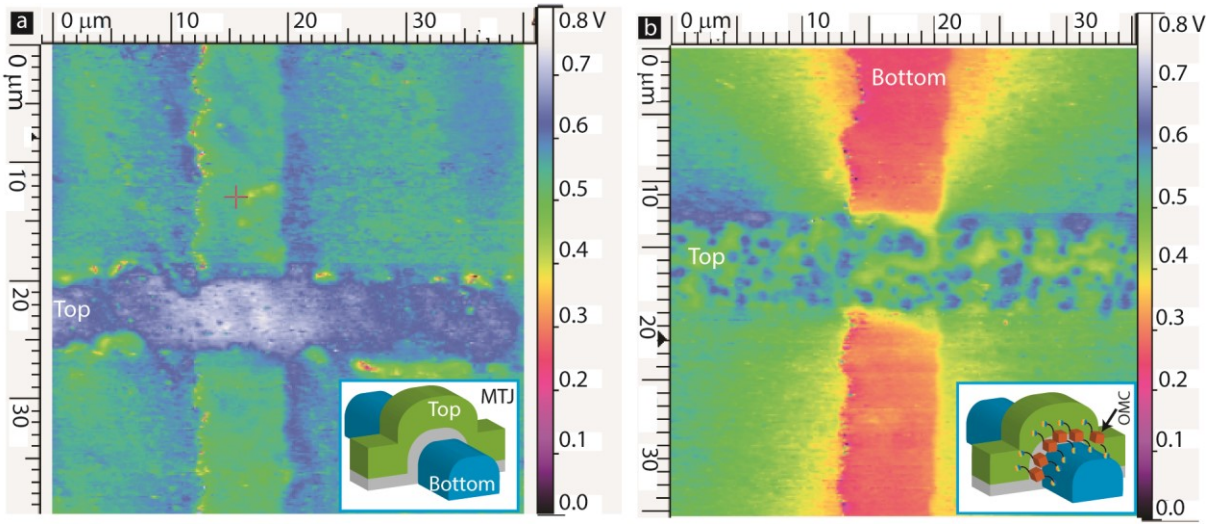

Fig. 8: KPAFM image of (a) MTJ and (b) MTJMSD.

To investigate the impact of OMCs on the MTJ junction area-specific magnetic properties, we studied an array of thousands of MTJs. An array of MTJ cylinders were transformed into MTJMSDs by bridging the OMC channels across the AlOx insulator. Topography imaging confirmed the physical presence of MTJMSD pillars. However, at the corresponding physical locations, the MTJMSD's MFM contrast was negligible. We occasionally observed high MFM contrast at MTMSD sites. This high contrast MFM is believed to be an unaffected MTJ or failed MTJMSD, where OMCs did not produce strong coupling. An in-depth discussion about the MFM study on an array of MTJs is presented elsewhere [11]. In conclusion, the MFM studies provide direct evidence that OMCs were able to impact the large area of MTJs at room temperature. In the case of MTJMSD with cross patterns, OMCs are expected to impact ferromagnetic electrodes beyond the MTJ junction areas as observed in the MFM images shown in Fig. 7b-c.

Our MFM studies indicated the OMCs produced a long-range effect on ferromagnetic electrodes (Fig. 7). We hypothesize that such large-scale OMC induced magnetic changes must also be observed in other types of experimental studies measuring different properties such as optical absorption and work function. To further confirm the OMC impact, we also conducted Kelvin Probe Atomic Force Microscopy (KPAFM) on MTJMSDs (Fig. 8). KPAFM of the bare MTJ, without OMCs, showed a moderate difference of ~0.2 V in surface potentials of the top and bottom ferromagnets. However, an MTJ produced in the same batch showed a very different response after hosting OMC channels to become an MTJMSD. The bottom electrode's surface potential was ~0.4-0.6 V lower than the surface potential of the top ferromagnetic electrode. The significant difference in surface potential is attributed to the OMC induced rearrangement of the density of electrons on the MTJMSD. KPAFM study also supports the MFM studies that OMCs produce a long-range effect on the ferromagnetic electrodes' properties.

In the case of MTJMSD based solar cells, one needs to focus on identifying the material (OMC or ferromagnetic electrodes) responsible for light absorption. Based on the experimental results we observed we need > 25 μm^2 area to absorb light radiation necessary to create power generation reported in this paper. It is noteworthy that OMCs are unable to produce enough surface area in the MTJMSD for capturing light radiation. The actual area of OMCs making bridges between the two ferromagnetic electrodes is roughly 3 nm x 10 μm= 0.03 μm^2. OMCs at any other places do not make any contribution in MTJMSD [11]. Hence, estimated effective OMC area is two orders of magnitude smaller than the required area, and hence OMC cannot absorb the required number of photons to produce observed solar power from MTJMSDs. To ensure the OMC indeed made a bare MTJ light-sensitive, we conducted a Raman study. Raman study could evaluate our assumption that light absorption occurs on the MTJMSD junction, i.e., OMC impacted ferromagnetic electrodes. Raman study is capable of (a) measuring the bandgap of light-absorbing materials and (b) identifying new phases that develop on material films.

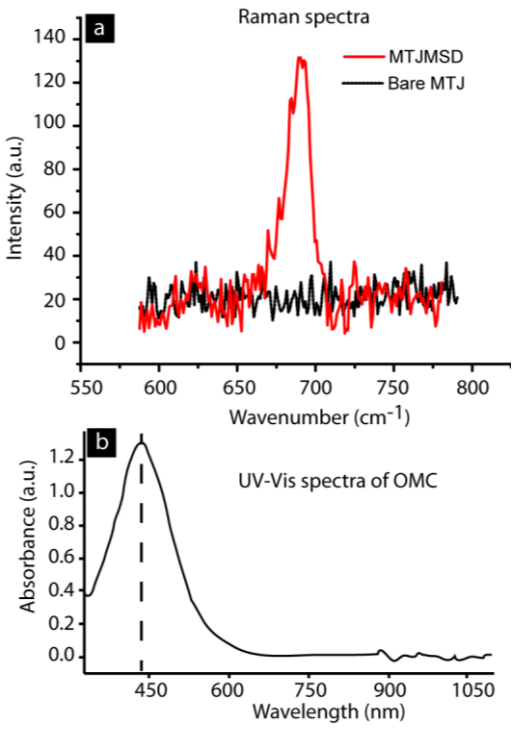

Fig. 9: (a) RAMAN spectra of MTJMSD and bare MTJ (b) UV-Vis spectra of OMC.

We conducted Raman using 785 nm laser on an MTJMSD and bare MTJ (Fig. 9a). Raman spectra were recorded from the cross-junction area. We did not observe any noticeable signal in the Raman spectra for MTJ that we could attribute to the ferromagnetic leads or the tunnel junction (Fig. 9). However, MTJMSD's junction produced a prominent signal around 687 cm^{-1} wavenumbers. This wavenumber corresponds to 14556 nm wavelength or ~85 meV energy. We do not believe this Raman response is due to any oxide formation because our MTJs were not heated beyond 95 °C. We demonstrated that on NiFe(80% Ni-20%Fe) acute oxidation start after 95 °C[15]. The Raman peak for the nickel oxide occurs around 590 cm^{-1} [26]. However, iron oxides are reported to exhibit multiple peaks; one of them was around 670 cm^{-1} [27]. However, iron is only 20% of the NiFe, and the only surface may contain sub-nm level iron oxide that is beyond the sensitivity range of Raman. Hence, it is not expected that the peak we observed in the Raman spectra is associated with any oxide formation. Also, bare MTJ processed in parallel to the sample studied here did not show any peak under identical Raman experiment condition. Our Raman study provides direct evidence that the OMC impacted MTJMSD and made the junction responsive to the

light radiation. Coincidently, the thermal activation energy barrier (~82±11 meV) calculated from the temperature-dependent current-voltage studies in the medium current state was comparable to the order of light energy (~85 meV) corresponding to Raman peak. We surmise that MTJMSD possesses an energy band gap of ~80 meV and hence capable of absorbing light radiation with energy ≥ the MTJMSD's bandgap.

We also do not believe that observed Raman arose from OMC. We also conducted spectroscopic absorbance of OMCs solution by utilizing UV-Vis spectrometer to investigate OMC's light absorption characteristics. For this study, we used Thermo scientific UV-Vis spectrometer. OMC produced a strong absorbance peak around 432 nm (Fig.9b). The OMC's absorbance peak at 432 nm wavelength suggests the light energy should be of the order of ~2.8 eV. OMC radiation absorbance energy (~ 2.8 eV) do not match with the MTJMSD radiation absorbance around ~85 meV. It must be noteworthy that our temperature vs. current-voltage study, discussed elsewhere in this paper, also yielded ~80 meV thermal energy barrier. Hence, MTJMSD's thermal energy barrier is in close agreement with the Raman data on MTJMSD.

Two fundamental properties of a solar cell are that it should be able to absorb light to create the population of opposite charges/spins and subsequently separate them to generate current and voltage[25]. Raman study suggest that MTJMSD's can absorb light radiation energy and produce photogenerated spin or charges. Our KPAFM study suggests that MTJMSDs two metallic leads are at significantly different surface potential and may be associated with a viable mechanism to separate photogenerated spins to produce the observed photovoltaic effect in this paper. We currently do not have exact understanding behind the observed spin-photovoltaic effect with MTJMSD. However, we have carried out extensive modelling of the observed experimental transport data to learn about the MTJMSD. We have mainly used tunneling models to understand MTJMSD properties in different current states and presented a hypothetical model in the supplementary material (Supplementary Material). By no means, we claim that our approach of utilizing tunneling models as a perfect method of investigating mechanistic insight behind the MTJMSD's spin-photovoltaic effect. However, it provides reasonable hints about the MTJMSD's state and OMC impact on barrier heights and thickness. Tunneling model does not incorporate the effect of temperature, magnetic anisotropies, and various forms of exchange couplings, e.g., biquadratic coupling and dipolar coupling. Hence, more accurate simulation and modeling are needed for better comprehension of spin-photovoltaic mechanism mentioned in this paper.

CONCLUSIONS: In this paper, we demonstrated the photovoltaic effect on MTJ based molecular spintronic devices (MTJMSDs). MTJMSDs exhibited three different current states termed as high (μA), medium (nA), and low (pA). In each state, light radiation produced the photovoltaic effect. OMC molecule appears to create robust exchange coupling between the two ferromagnetic electrodes of the magnetic tunnel junctions leading to significant changes in the electrical, magnetic, and optical properties of the ferromagnetic electrodes. OMC induced changes in the ferromagnetic electrodes also propagated outside the MTJ's perimeter. Magnetic studies, KPAFM, and Raman studies suggested that OMC transformed a ferromagnetic film into photoresponsive material and produced a built-in potential in the MTJMSD. MTJMSD's ability to absorb white light radiation and the ability to separate opposite spins in the three different current states lead to the net photovoltaic effect. MTJMSD's photovoltaic response responded to the magnetic field. This paper mainly reports the experimental observations.
Further investigation about the more profound understanding of the spin-photovoltaic effect is needed. We were also not able to provide an exact estimate of the energy conversion efficiency. It was experimentally challenging to determine the exact area responding to light radiation. Future work may focus on simultaneous KPAFM, MFM, and I-V measurements under dark and light for further understanding and new insights.

ACKNOWLEDGEMENT: Pawan Tyagi thanks Dr. Bruce Hinds and Department of Chemical and Materials engineering at University of Kentucky for facilitating experimental work on MTJMSD during his PhD. PT thanks Dr. Stephen Holmes and his postdoctoral scholar Dr. D.F. Li for producing OMC. An

aged OMC batch was used for conducting Raman, UV-VIS, and KPAFM study. We thank Dr. Carlos Morillo of Jasco for the Raman study. KPAFM and MFM of MTJMSD in the high current state were completed by Christopher Riso. The preparation of this paper was in part supported by National Science Foundation-CREST Award (Contract # HRD- 1914751), Department of Energy/ National Nuclear Security Agency (DE-FOA-0002013), and Air Force Office of Sponsored Research (Award #FA9550-13-1-0152). Any opinions, findings, and conclusions expressed in this paper are those of the author(s) and do not necessarily reflect the views of any funding agency and corresponding author's past and present affiliations.

REFERENCES

1. F. Hekking and Y. V. Nazarov, Physical Review B **44** (20), 11506 (1991).
2. I. Žutić, J. Fabian and S. D. Sarma, Phy. Rev. Lett. **88** (6), 066603 (2002).
3. I. Zutic and J. Fabian Materials Transactions **44** (10), 2062-2065 (2003).
4. B. Endres, M. Ciorga, M. Schmid, M. Utz, D. Bougeard, D. Weiss, G. Bayreuther and C. H. Back, Nature Communications **4**, 2068 (2013).
5. T. Kondo, J.-j. Hayafuji and H. Munekata, Japanese journal of applied physics **45** (7L), L663 (2006).
6. Y. V. Pershin and C. Piermarocchi, Physical Review B **72** (19), 195340 (2005).
7. A. Fedorov, Y. V. Pershin and C. Piermarocchi, Phys. Rev. B **72** (24), 245327 (2005).
8. L. Fedichkin, V. Ryzhii and V. V'yurkov, Journal of Physics: Condensed Matter **5** (33), 6091 (1993).
9. F. Bottegoni, M. Celebrano, M. Bollani, P. Biagioni, G. Isella, F. Ciccacci and M. Finazzi, Nat. Mater. **13**, 790 (2014).
10. X. N. Sun, S. Velez, A. Atxabal, A. Bedoya-Pinto, S. Parui, X. W. Zhu, R. Llopis, F. Casanova and L. E. Hueso, Science **357** (6352), 677-+ (2017).
11. P. Tyagi, C. Baker and C. D'Angelo, Nanotechnology **26**, 305602 (2015).
12. P. Tyagi and T. Goulet, MRS Comm., 1-5 (2018).
13. P. Tyagi, C. Riso and E. Friebe, Organic Electronics **64**, 188-194 (2019).
14. P. Tyagi, D. F. Li, S. M. Holmes and B. J. Hinds, J. Am. Chem. Soc. **129** (16), 4929-4938 (2007).
15. P. Tyagi, E. Friebe and C. Baker, J.Nanoparticle Res. **17** (11), 452 (2015).
16. P. Tyagi, E. Friebe and C. Baker, NANO **10** (3), 1530002 (2015).
17. P. Tyagi, J. Nanoparticle Res. **14** (10), 1195 (2012).
18. D. F. Li, S. Parkin, G. B. Wang, G. T. Yee, R. Clerac, W. Wernsdorfer and S. M. Holmes, J. Am. Chem. Soc. **128** (13), 4214-4215 (2006).
19. K. Park and H. S. M., Phys. Rev. B **74**, 224440 (2006).
20. P. Tyagi and E. Friebe, J. Mag. Mag. Mat. **453**, 186-192 (2018).
21. J. S. Moodera, J. Nassar and G. Mathon, Ann. Rev. Mater. Sci. **29**, 381-432 (1999).
22. B. Hu, J. Yao and B. J. Hinds, App. Phys. Lett. **97** (20), 203111 (2010).
23. B. Hu and B. J. Hinds, IEEE Trans. Nanotech. **11** (6), 1073-1079 (2012).
24. S. R. Smith and R. L. McCreery, Advanced Electronic Materials **4** (5), 1800093 (2018).
25. S. M. Sze and K. K. Ng, *Physics of semiconductor devices*. (John wiley & sons, 2006).
26. C. Mrabet, M. B. Amor, A. Boukhachem, M. Amlouk and T. Manoubi, Ceramics International **42** (5), 5963-5978 (2016).
27. Y.-S. Li, J. S. Church and A. L. Woodhead, J. Mag. Mag. Mat. **324** (8), 1543-1550 (2012).